Ceramics International 46 (2020) 21336–21342

Contents lists available at ScienceDirect

Ceramics International

journal homepage: www.elsevier.com/locate/ceramint

Effects of W^{6+} substitution on crystal structure and microwave dielectric properties of $Li_3Mg_2NbO_6$ ceramics

Ping Zhang[a,*], Manman Hao[a], Xurui Mao[b,**], Kexin Sun[a], Mi Xiao[a]

[a] School of Electrical and Information Engineering and Key Laboratory of Advanced Ceramics and Machining Technology of Ministry of Education, Tianjin University, Tianjin, 300072, PR China

[b] State Key Laboratory on Integrated Optoelectronics, Institute of Semiconductors, Chinese Academy of Sciences, Beijing, 100083, PR China

ARTICLE INFO

Keywords:
$Li_3Mg_2(Nb_{1-x}W_x)O_{6+x/2}$
Polarizability
Average bond valence
Bond energy

ABSTRACT

$Li_3Mg_2(Nb_{1-x}W_x)O_{6+x/2}$ ($0 \le x \le 0.08$) ceramics were synthesized by the solid-state reaction route. The effects of W^{6+} substitution on the phase composition, microstructure and microwave dielectric properties of $Li_3Mg_2NbO_6$ ceramics were investigated systematically. The XRD results showed that all the samples formed a pure solid solution in the whole doping range. The SEM iamges and relative density revealed the dense structure of $Li_3Mg_2(Nb_{1-x}W_x)O_{6+x/2}$ ceramics. The relationship between the crystal structure and dielectric properties of $Li_3Mg_2(Nb_{1-x}W_x)O_{6+x/2}$ ceramics was researched through polarizability, average bond valence, and bond energy. The substitution of W^{6+} for Nb^{5+} in $Li_3Mg_2(Nb_{1-x}W_x)O_{6+x/2}$ ceramics significantly promoted the $Q \times f$ values. In addition, the increase of W^{6+} content improved the thermal stability of the $Li_3Mg_2(Nb_{1-x}W_x)O_{6+x/2}$ ceramics. The $Li_3Mg_2(Nb_{0.94}W_{0.06})O_{6.03}$ ceramics sintered at 1175 °C for 6h possessed excellent properties: $\varepsilon_r \sim$ 15.82, $Q \times f \sim$ 124,187 GHz, $\tau_f \sim -18.28$ ppm/°C.

1. Introduction

In the age of information technology, microwave dielectric ceramics play an important role in daily life, national defense, and military. The high frequency, miniaturization and low cost of microwave devices have become the mainstream of microwave technology. Microwave dielectric ceramics are widely used as key materials for passive components in microwave communication systems, such as filters, capacitors, resonators, dielectric antennas, and dielectric waveguides [1–6]. In recent years, the new microwave dielectric ceramic materials have emerged endlessly. However, comprehensive properties of most materials cannot meet the requirements of practical applications. Therefore, the research and exploration of ceramic materials with excellent dielectric properties is the mainstream direction of the times. Dielectric ceramics with different characteristics have different applications. Materials with low dielectric constant characteristics can reduce the delay of signal transmission. Materials with high quality factor characteristics can reduce the power loss of the system. Dielectric ceramics with a temperature coefficient close to zero can improve the thermal stability of the system. In addition, when the sintering temperature is lower than 950 °C, ceramic materials can be co-fired with the silver electrodes [7–9].

In recent years, the $Li_3Mg_2NbO_6$ ceramics with orthorhombic structure had attracted more and more attention due to its excellent dielectric properties. In 2009, Yuan et al. [1] reported for the first time $Li_3Mg_2NbO_6$ ceramics with excellent dielectric properties. Zhao et al. [10] studied the effects of Ca^{2+}, Ni^{2+}, Zn^{2+}, and Mn^{2+} on dielectric properties of $Li_3Mg_2NbO_6$ ceramics. Later, Zhang et al. [11,12] reported that $Li_3(Mg_{0.98}Mn_{0.02})_2NbO_6$ and $Li_3(Mg_{1-x}Ni_x)_2NbO_6$ ceramics have higher $Q \times f$ values. Xing et al. [13] researched the effect of Co^{2+} on dielectric properties of $Li_3Mg_2NbO_6$ ceramics. M. Castellanos and Zhang et al. [14,15] researched the effect of replacing Nb^{5+} on dielectric properties of $Li_3Mg_2NbO_6$ ceramics. Wang et al. [16] reported the $Li_3Mg_2Nb_{1-x}V_xO_6$ ($x = 0.02$) ceramics sintered at 900 °C displayed outstanding dielectric properties:$\varepsilon_r \sim 16$, $Q \times f \sim$ 131,000 GHz and $\tau_f \sim -26$ ppm/°C. In addition, Wang et al. [17] systematically studied the effect of Ta^{5+} substitution on the structure and dielectric properties of $Li_3Mg_2NbO_6$ ceramics. The $Li_3Mg_2Nb_{0.98}Ta_{0.02}O_6$ ceramics had outstanding dielectric properties: $\varepsilon_r \sim 15.58$. $Q \times f \sim$113,000 GHz and $\tau_f \sim -4.5$ ppm/°C.

However, so far, there has been little discussion about the dielectric properties of $Li_3Mg_2NbO_6$ ceramics with hexavalent ions replacing Nb^{5+}. Zhang et al. [18] greatly reduced the dielectric loss of $Ba_3ZnNb_2O_9$ ceramics by replacing Nb^{5+} with Mo^{6+}. In addition,

* Corresponding author.
** Corresponding author.
E-mail addresses: zptai@163.com (P. Zhang), maoxurui@semi.ac.cn (X. Mao).

https://doi.org/10.1016/j.ceramint.2020.05.229
Received 25 March 2020; Received in revised form 30 April 2020; Accepted 20 May 2020
Available online 26 May 2020
0272-8842/ © 2020 Elsevier Ltd and Techna Group S.r.l. All rights reserved.

$Li_3Mg_2(Nb_{0.98}Mo_{0.02})O_{6.01}$ ceramics [19] had the best microwave dielectric properties when sintered at 1200 °C for 6h, $\varepsilon_r \sim 15.18$, $Q \times f \sim 116{,}266$ GHz, $\tau_f \sim -15.71$ ppm/°C. Zhang et al. [20] analyzed in detail the correlation between the sintering characteristics and microwave dielectric properties of $Li_{3+x}Mg_2Nb_{1-x}Ti_xO_6$ ($0.02 \le x \le 0.08$) ceramics. In addition, Wang et al. [21] systematically studied the effect of Ti^{4+} substitution on the structure and dielectric properties of $Li_3Mg_2NbO_6$ ceramics. The $Li_3Mg_2Nb_{0.96}Ti_{0.04}O_{5.98}$ ceramics showed excellent dielectric properties: $\varepsilon_r \sim 15.88$. $Q \times f \sim 131{,}000$ GHz and $\tau_f \sim -26.8$ ppm/°C. Wu et al. [22] replaced Nb^{5+} with W^{6+} significantly reduced the dielectric loss of $Ba(Zn_{1/3}Nb_{2/3})O_3$ ceramics. W^{6+} and Nb^{5+} have similar ion radii, so W^{6+} can be used to replace the Nb^{5+} of $Li_3Mg_2NbO_6$ ceramics. The volatilization of lithium element can cause the charge transfer of neutral ceramics. In order to maintain electrical neutrality, oxygen vacancies will be generated, which will affect the microwave dielectric properties of ceramics. The oxygen ions introduced by WO_3 can maintain the electrical neutrality of $Li_3Mg_2NbO_6$ ceramics and reduce the oxygen vacancies, thereby improving the performance of the ceramics.

In this paper, $Li_3Mg_2(Nb_{1-x}W_x)O_{6+x/2}$ ($0 \le x \le 0.08$) ceramics were synthesized via the solid-state reaction route. The sintering characteristics, dielectric properties, and crystal structure of $Li_3Mg_2(Nb_{1-x}W_x)O_{6+x/2}$ ($0 \le x \le 0.08$) ceramics were systematically researched.

2. Experimental section

The powder was prepared by mixing Nb_2O_5 (99.9%), Li_2CO_3 (97%), WO_3 (99.9%), MgO (99.9%) as raw materials according to $Li_3Mg_2(Nb_{1-x}W_x)O_{6+x/2}$ ($0 \le x \le 0.08$) formula. The prepared powder mixture was poured into a nylon tank filled with deionized water and ground for 8h. The ground mixture was calcined for 4h at 950 °C after drying. Repeat the above ball milling and drying steps. The powder mixture mixed with 8 wt% paraffin, and pressed at 4 MPa to make a cylinder with a cylinder (~10 mm in diameter and ~5 mm in height). It was sintered at a temperature of 1100 °C–1200 °C for 6h to obtain $Li_3Mg_2(Nb_{1-x}W_x)O_{6+x/2}$ ($0 \le x \le 0.08$) ceramics.In order to reduce the evaporation of the lithium element during the whole sintering process at high temperature, the pressed green body was placed on the ZrO_2 plate according to the structure shown in Fig. 1.

The Rigaku D/max 2550 PC was used to detect the phase composition and crystal structure of $Li_3Mg_2(Nb_{1-x}W_x)O_{6+x/2}$ ($0 \le x \le 0.08$) ceramics. XRD results were obtained through a step-scan method at a speed of 0.02°/s between 15° and 70°(2θ). The microstructure of the samples was characterized using a scanning electron microscope (ZEISS MERLIN Compact, Germany). The grain size distributions were calculated by Nano Measurer software. The bulk density of all samples was obtained by the Archimedes method. A vector network analyzer was used to test the microwave dielectric properties of the samples (N5234A, Agilent Co, America). The open-cavity method measured the dielectric resonance frequency, and the closed-cavity method measured the center resonance frequency, the on-load quality factor, and the insertion loss in TE_{011} mode [23,24]. In the temperature range of 25 °C–85 °C, the value of τ_f was calculated by the following formula:

$$\tau f = \frac{f85 - f25}{f25(T85 - T25)} \times 10^6 (ppm/°C) \quad (1)$$

where f_{85} and f_{25} represented the resonant frequencies at the temperature of T_{85} and T_{25}, respectively.

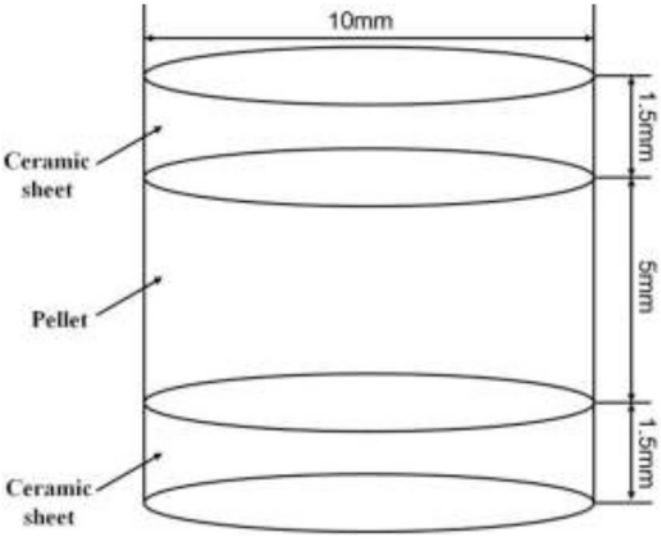

Fig. 1. Ceramic stacking method.

3. Results and discussion

Fig. 2 shows the X-ray diffraction patterns of $Li_3Mg_2(Nb_{1-x}W_x)O_{6+x/2}$ ceramics sintered at 1175 °C. The diffraction peaks of all the samples match the standard card (JCPDS#86–0346), indicating that all the samples obtained in this experimental section are pure phases. The XRD diffraction patterns of the samples obtained by replacing Nb^{5+} with W^{6+} in $Li_3Mg_2NbO_6$ ceramics have no other diffraction peaks, indicating that solid solutions are formed within the experimental range. In addition, Fig. 2 (b) shows that the diffraction peak shifts to a high angle as the content of W^{6+} increases, which indicates the unit cell volume decreases. The radius of W^{6+} (0.60 Å) is smaller than the radius of Nb^{5+} (0.64 Å). As the amount of W^{6+} increases, the cell volume becomes smaller and smaller [25]. The lattice parameters after the Rietveld refinements are listed in Table 1. It can be seen from Table 1 that as the content of W^{6+} increases, the cell volume of the sample gradually decreases, which is consistent with the results of Fig. 2.

Fig. 3 shows the SEM images of $Li_3Mg_2(Nb_{1-x}W_x)O_{6+x/2}$ ceramics sintered at 1175 °C. The surface of all samples is dense. The results show that the proper amount of W^{6+} can promote the grain growth of $Li_3Mg_2NbO_6$ ceramics and increase the densification of the ceramics. However, the growth of grains will be inhibited when the doping amount exceeds a certain limit. When $x = 0.08$, the structure at the grain boundaries is loose and a phenomenon similar to melting occurs. This is because excessive W^{6+} can reduce the sintering temperature of $Li_3Mg_2(Nb_{1-x}W_x)O_{6+x/2}$ ceramics. The histograms of grain sizes are shown in Fig. 4. The calculation results of the average grain size in Fig. 4 are ~31.6 μm, ~33.78 μm, ~36.76 μm, ~42.87 μm and ~37.82 μm, respectively. The grain sizes are closely related to the content of W^{6+}. When $x \le 0.06$, the grain sizes increase with the increase of W^{6+} content. When $0.06 < x \le 0.08$, the grain sizes decrease significantly. With the emergence of small-sized grains, the number of grain boundaries increases, and the grain boundaries with two-dimensional defects degrade the dielectric properties of $Li_3Mg_2(Nb_{1-x}W_x)O_{6+x/2}$ ceramics [26]. Therefore, as the W^{6+} content increases, the sintering temperature of the $Li_3Mg_2(Nb_{1-x}W_x)O_{6+x/2}$ ceramics should be appropriately reduced.

Fig. 5 shows the relative density, dielectric constant (ε_r) and $Q \times f$ values of $Li_3Mg_2(Nb_{1-x}W_x)O_{6+x/2}$ ceramics sintered at different sintering temperatures. Fig. 5 (a) shows that the relative density curve of $Li_3Mg_2(Nb_{1-x}W_x)O_{6+x/2}$ ceramics. The change trend of relative density matches well with the SEM pictures where the uneven particle size and pores lead to the low density. The relative density of all samples increase rapidly as the sintering temperature increase from 1100 °C to 1175 °C. The relative density of $Li_3Mg_2(Nb_{1-x}W_x)O_{6+x/2}$ ceramics sintered at 1100 °C–1200 °C for 6h is greater than 95%. Further raising the temperature would reduce the density slightly. Within the solid solution limit of W^{6+}, it is more and more beneficial to promote the sintering of samples with the increase of W^{6+} content. Maintaining the original sintering temperature of $Li_3Mg_2(Nb_{1-x}W_x)O_{6+x/2}$ ceramics will cause

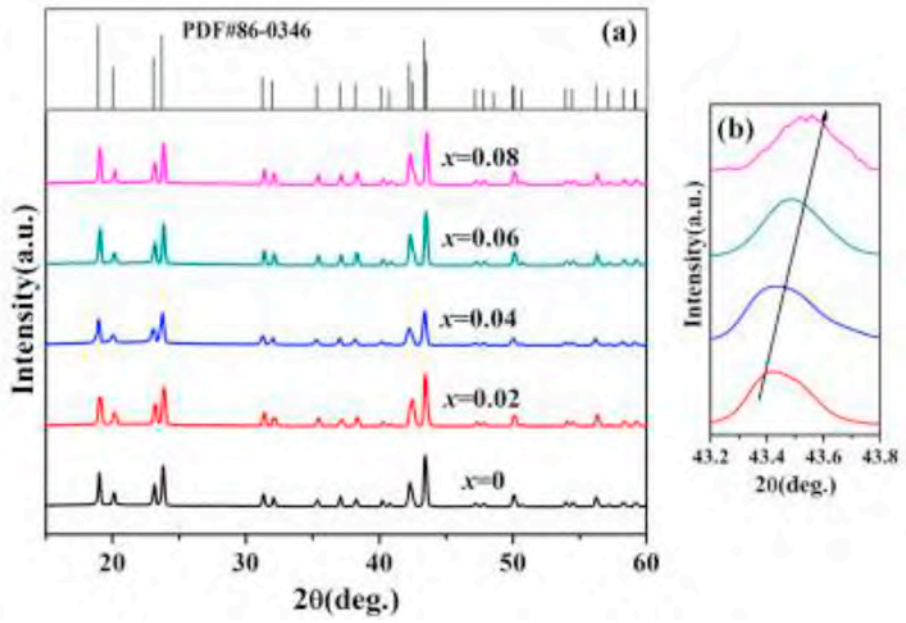

Fig. 2. The X-ray diffraction patterns of $Li_3Mg_2(Nb_{1-x}W_x)O_{6+x/2}$ ($0 \le x \le 0.08$) ceramics sintered at 1175 °C.

Table 1
Crystallographic structures of $Li_3Mg_2(Nb_{1-x}W_x)O_{6+x/2}$ ($0 \le x \le 0.08$) ceramics sintered at 1175 °C for 6h.

x	a	b	c	α = β = γ	V(Å)	ρ_{re}(g/cm^3)
0	5.8957	8.5590	17.7196	90°	894.15	3.830
0.02	5.8934	8.5585	17.7182	90°	892.11	3.834
0.04	5.8896	8.5563	17.7074	90°	891.94	3.839
0.06	5.5883	8.5541	17.7047	90°	891.61	3.842
0.08	5.8843	8.5523	17.7028	90°	891.43	3.846

over-firing. Therefore, the sintering temperature should be reduced. Fig. 5 (b) shows that the dielectric constant changes approximately the same as the relative density, which indicates that density is one of the main factors affecting the dielectric constant of $Li_3Mg_2(Nb_{1-x}W_x)O_{6+x/2}$ ceramics. Fig. 5 (c) shows the $Q \times f$ values of $Li_3Mg_2(Nb_{1-x}W_x)O_{6+x/2}$ ceramics sintered at different sintering temperatures.. The $Q \times f$ values of all samples show a trend of increasing first and then decreasing with the increase of sintering temperature, which is roughly consistent with the change of relative density. When $x \le 0.06$, $Li_3Mg_2(Nb_{1-x}W_x)O_{6+x/2}$ ceramics sintered at 1175 °C have the largest $Q \times f$ value. When $x = 0.08$, the optimal sintering temperature of $Li_3Mg_2(Nb_{1-x}W_x)O_{6+x/2}$ ceramics is 1150 °C. This indicates that the optimal sintering temperature of $Li_3Mg_2(Nb_{1-x}W_x)O_{6+x/2}$ ceramics decreases with the increase of W^{6+} content, which is consistent with the analysis results of the SEM images.

The dielectric constant of pure-phase ceramics is mainly related to density and ionic polarizability [27]. The results of phase analysis show that the $Li_3Mg_2(Nb_{1-x}W_x)O_{6+x/2}$ ceramics obtained in this study are pure phases. Therefore, the effect of the second phase on dielectric constant is negligible. Ionic polarizability and density are the main

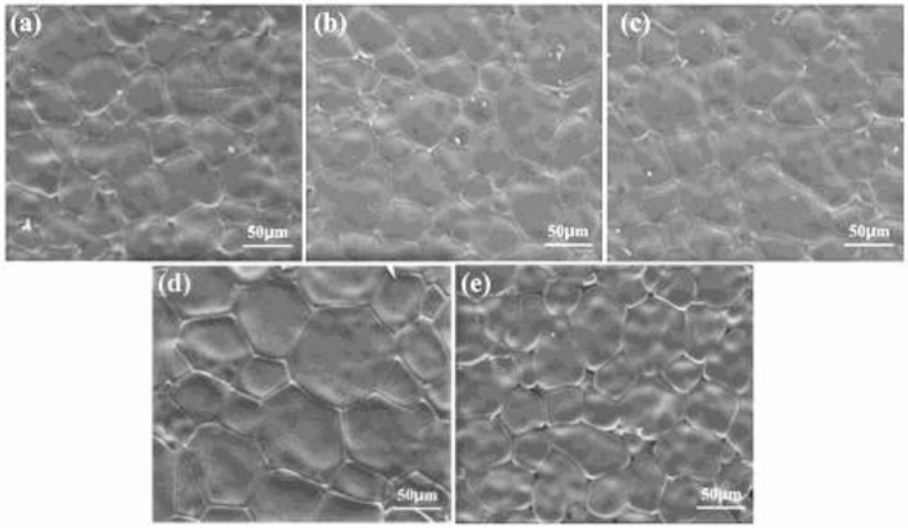

Fig. 3. The surface microstructures of $Li_3Mg_2(Nb_{1-x}W_x)O_{6+x/2}$ ($0 \le x \le 0.08$) ceramics sintered at 1175 °C: (a) x = 0, (b) x = 0.02, (c) x = 0.04, (d) x = 0.06, (e) x = 0.08.

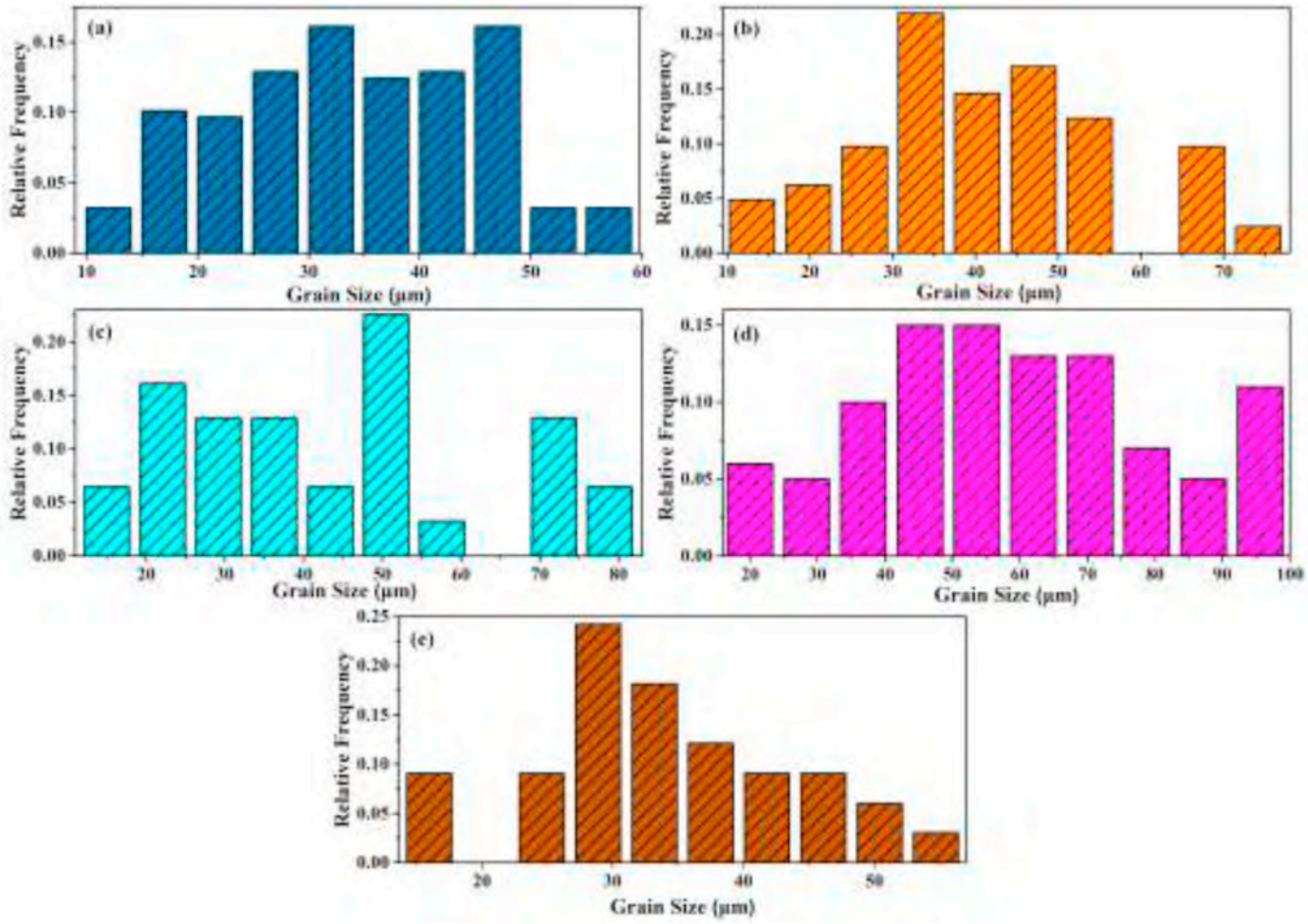

Fig. 4. Grain size distribution of $Li_3Mg_2(Nb_{1-x}W_x)O_{6+x/2}$ ($0 \le x \le 0.08$) ceramics sintered at 1175 °C: (a) x = 0, (b) x = 0.02, (c) x = 0.04, (d) x = 0.06, (e) x = 0.08.

factors affecting dielectric constant in this experiment. The porosity-corrected dielectric constant (ε_{pc}) obtained from equation (2) further shows the relationship between the ion polarization and the dielectric constant:

$$\varepsilon_r = \varepsilon_{pc}\left(1 - \frac{3p(\varepsilon_{pc}-1)}{2\varepsilon_{pc}+1}\right) \tag{2}$$

where ε_r and p are the measured dielectric constant and porosity, respectively. The actual dielectric polarization (α_{obs}) can be obtained according to the dielectric constant of the Clausius-Mossotti:

$$\alpha_{obs} = \frac{3V_m(\varepsilon_{pc}-1)}{4\pi(\varepsilon_{pc}+2)} \tag{3}$$

where the V_m is the unit cell volume. The theoretical ion polarizability (α_{theo}) can be obtained from the following formula [28]:

$$\alpha_{theo} = 3\alpha_{Li^+} + 2\alpha_{Mg^{2+}} + (1-x)\alpha_{Nb^{5+}} + x\alpha_{W^{6+}} + (6 + x/2)\alpha_{O^{2-}} \tag{4}$$

Table 2 lists the porosity-corrected dielectric constant of $Li_3Mg_2(Nb_{1-x}W_x)O_{6+x/2}$ ceramics sintering at 1175 °C for 6h. Fig. 6 shows the relationship between the actual dielectric constant (ε_r) and ε_{pc}. It can be seen from Fig. 6 and Table 2, the change of the ε_r is the same as that of ε_{pc}. When $x \le 0.6$, ε_r and ε_{pc} increase with the increase of W^{6+} content. The ε_r and α_{theo} increase with the increase of x. When $x > 0.6$, the ionic polarizability continues to increase, while the ε_r begins to decrease. This phenomenon shows that when $x > 0.6$, the effect of density on the dielectric constant of $Li_3Mg_2(Nb_{1-x}W_x)O_{6+x/2}$ ceramics is greater than ionic polarization. The ε_r decreases as the relative density of the sample decreases [29–31].

The dielectric loss of the sample was significantly lower than that of $Li_3Mg_2NbO_6$ ceramics in the research by Yuan et al. [1]. Generally, intrinsic and extrinsic factors determine the $Q \times f$ values of ceramics. Intrinsic losses are involved with the lattice structure, while extrinsic losses are usually involved with the second phase, porosity, grain size, and impurities. The phase analysis results in Fig. 2 indicate that the $Li_3Mg_2(Nb_{1-x}W_x)O_{6+x/2}$ ceramics are pure phases. Therefore, the $Q \times f$ values mainly depend on the density and crystal structure [32]. The refinement results of XRD data and the crystal structure of the $Li_3Mg_2NbO_6$ ceramics are shown in Fig. 7. As shown in Fig. 7, the $Li_3Mg_2NbO_6$ ceramics include four kinds of oxygen octahedra: Li1|$Mg1O_6$, Li2|$Mg2O_6$, Li3|$Mg3O_6$, and NbO_6. The bond valence (V_i) of $Li_3Mg_2(Nb_{1-x}W_x)O_{6+x/2}$ ceramics sintered at 1175 °C in different oxygen octahedra can be calculated by the following formula:

$$v_{i-o} = \exp\left[\frac{R_{i-o} - d_{i-o}}{b}\right] \tag{5}$$

$$V_i = \sum v_{i-o} \tag{6}$$

where the $R_{i\text{-}o}$ and $d_{i\text{-}o}$ are the bond valence parameters of the oxygen octahedron, respectively. b is constant (0.37 Å). The bond valences of $Li_3Mg_2(Nb_{1-x}W_x)O_{6+x/2}$ ceramics sintered at 1175 °C for 6h are shown in Table 3. Fig. 8 is the relationship curve between the $Q \times f$ values, relative density and the average bond valence of $Li_3Mg_2(Nb_{1-x}W_x)O_{6+x/2}$ ceramics sintered at 1175 °C for 6h. In this work, the relative density

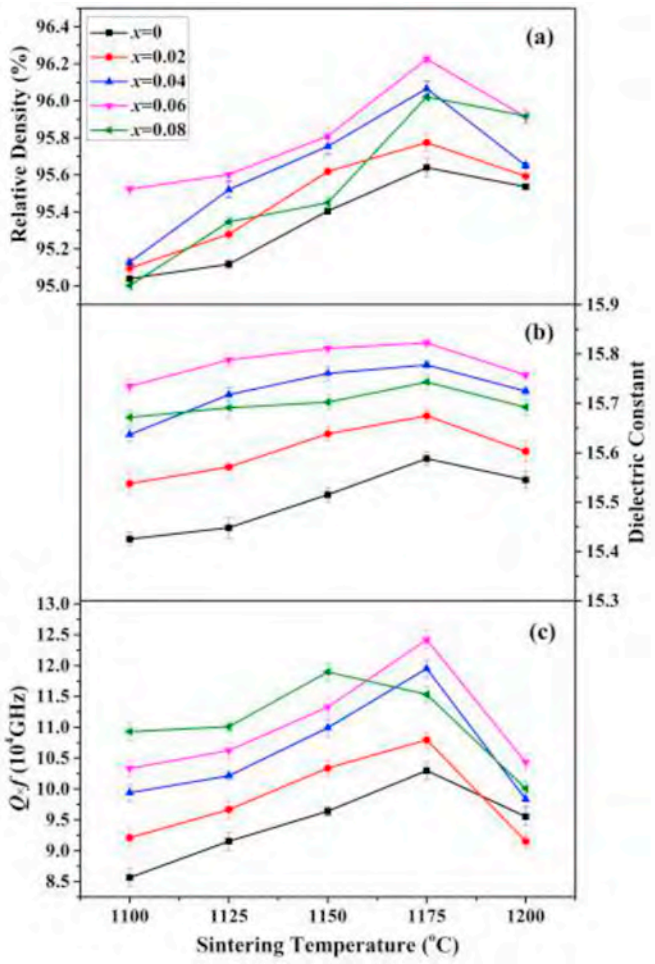

Fig. 5. The relative density, dielectric constant (ε_r), and $Q \times f$ values of $Li_3Mg_2(Nb_{1-x}W_x)O_{6+x/2}$ ($0 \le x \le 0.08$) ceramics sintered at various temperature for 6h.

Table 2
The detailed information of porosity-corrected dielectric constant (ε_{pc}) of $Li_3Mg_2(Nb_{1-x}W_x)O_{6+x/2}$ ($0 \le x \le 0.08$) ceramics sintered at 1175 °C for 6h

x value	α_{theo}	ε_{theo}	ε_{pc}	ε_r	p
0	22.27	16.1400	15.4997	15.5880	0.0436
0.02	22.2747	16.3716	15.7413	15.6746	0.0423
0.04	22.2794	16.4095	15.8213	15.7778	0.0393
0.06	22.2841	16.4646	15.8944	15.8226	0.0380
0.08	22.2888	16.5040	15.8936	15.7433	0.0406

of $Li_3Mg_2(Nb_{1-x}W_x)O_{6+x/2}$ ceramics sintered at 1175 °C for 6h is greater than 95%. When x = 0.06, the $Q \times f$ values reach a peak of ~124,187 GHz and then show a downward trend. Fig. 8 shows that the change trend of $Q \times f$ values is basically consistent with the relative density and average bond valence. It indicates the density and the average bond valence together determine the $Q \times f$ values of $Li_3Mg_2(Nb_{1-x}W_x)O_{6+x/2}$ ceramics.

The τ_f is used to characterize the degree of drift of the resonance frequency with temperature. In general, the octahedral distortions is one of the important influencing factors of τ_f values. The bond energy is the main influence factor of the octahedral distortions. Sanderson [33–35] reported that the bond energy was determined by electronegativity and chemical bonds. By formulas (7)-(12), the bond energy E of materials with complex components can be calculated:

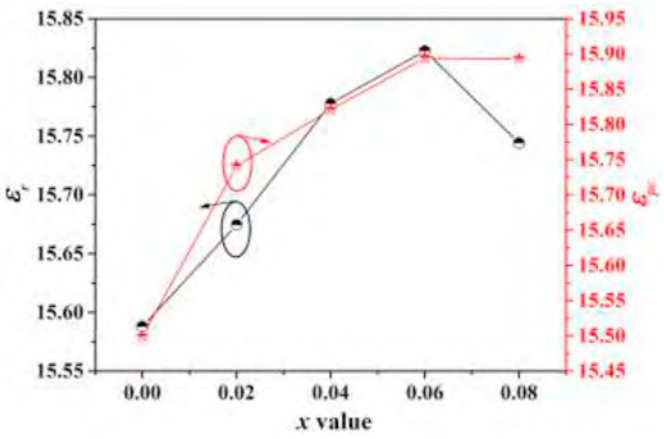

Fig. 6. The relationship between dielectric constant (ε_r) and porosity-corrected dielectric constant (ε_{pc}) of $Li_3Mg_2(Nb_{1-x}W_x)O_{6+x/2}$ ($0 \le x \le 0.08$) ceramics sintered at 1175 °C.

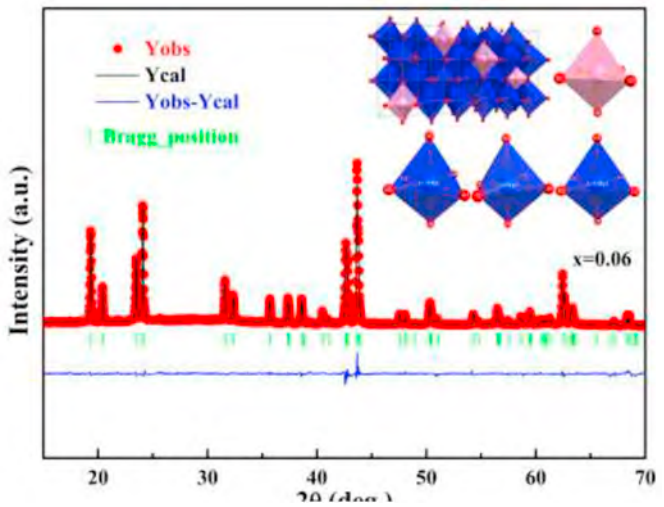

Fig. 7. The Rietveld refinement patterns of $Li_3Mg_2(Nb_{0.94}W_{0.06})O_{6.03}$ ceramics sintered at 1175 °C (the illustration shows the crystal structure of $Li_3Mg_2NbO_6$ ceramics).

$$E = \sum_{\mu} E_b^{\mu} \tag{7}$$

$$E_b^{\mu} = t_i E_i^{\mu} + t_c E_c^{\mu} \tag{8}$$

$$E_i^{\mu} = \frac{33200}{d^{\mu}} \tag{9}$$

$$E_c^{\mu} = \frac{(r_{cA} + r_{cB})}{d^{\mu}} (E_{hA-A} E_{hB-B})^{1/2} \tag{10}$$

$$t_i + t_c = 1 \tag{11}$$

$$t_i = \left| \frac{(S_A - S_B)/\Delta S_B}{2} \right| \tag{12}$$

where $E_b^{\mu}$is the bond energy of the μ bond, E_i^{μ} is the ion bond energy, E_c^{μ} is the non-polar covalent bond energy. t_i and t_c in formula (11) are the ion mixing coefficient and the covalent mixing coefficient, respectively. t_i can be obtained by the electronegativity of A and B ions (S_A and S_B). According to the above formula, Table 4 shows the calculation results of the bond energy of $Li_3Mg_2(Nb_{1-x}W_x)O_{6+x/2}$ ceramics. Fig. 9 is the relationship between the τ_f values and the total bond energy of $Li_3Mg_2(Nb_{1-x}W_x)O_{6+x/2}$ ceramics sintered at 1175 °C for 6h. Fig. 9 shows as x increases, the total bond energy also increases. It can be seen

Table 3
The bond valence of $Li_3Mg_2(Nb_{1-x}W_x)O_{6+x/2}$ ($0 \le x \le 0.08$) ceramics sintered at 1175 °C for 6h.

x value	Bond vanlence							
	Nb-O_6	(Li1|Mg1)O_6		(Li2|Mg2)O_6		(Li3|Mg3)O_6		Average
		$Li_{(1)}O_6$	$Mg_{(1)}O_6$	$Li_{(2)}O_6$	$Mg_{(2)}O_6$	$Li_{(3)}O_6$	$Mg_{(2)}O_6$	
0	4.81	1.17	2.07	1.19	2.06	1.12	2.03	1.98
0.02	4.94	1.19	2.06	1.19	2.05	1.19	2.09	2.06
0.04	5.21	1.18	2.07	1.20	2.06	1.09	2.06	2.12
0.06	5.56	1.19	2.08	1.19	2.04	1.18	2.11	2.18
0.08	5.59	1.18	2.02	1.16	1.95	0.97	1.99	2.15

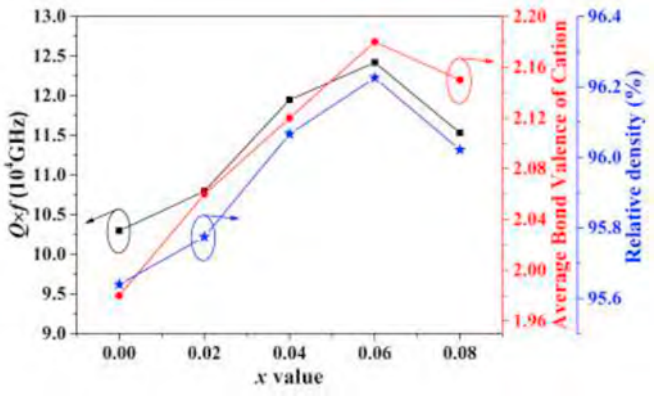

Fig. 8. The relationship between $Q \times f$ values, relative density and average bond valence of $Li_3Mg_2(Nb_{1-x}W_x)O_{6+x/2}$ ($0 \le x \le 0.08$) ceramics sintered at 1175 °C.

Table 4
The bond energy of $Li_3Mg_2(Nb_{1-x}W_x)O_{6+x/2}$ ($0 \le x \le 0.08$) ceramics sintered at 1175 °C for 6h.

Bond type	bong energy *E* (KJ/mol)				
	x = 0.00	x = 0.02	x = 0.04	x = 0.06	x = 0.08
Nb/W-O1	583.097	583.604	584.346	583.764	583.792
Nb/W-O2	546.503	546.683	548.048	550.384	547.837
Li1-O1	407.260	402.211	406.030	407.141	408.177
Li1-$O2^1$	383.719	390.111	375.815	391.484	391.889
Li1-$O2^2$	396.003	389.837	388.674	370.587	386.172
Li2-O1	394.634	391.613	382.733	394.187	393.535
Li2-$O2^1$	395.289	401.089	401.668	393.424	399.425
Li2-$O2^2$	393.982	394.000	396.247	397.380	380.914
Li3-O1	363.399	376.715	376.426	397.854	388.098
Li3-O2	408.597	406.347	416.434	404.887	404.376
Mg1-O1	288.509	284.932	287.638	288.565	287.159
Mg1-$O2^1$	271.832	276.360	275.676	277.463	277.698
Mg1-$O2^2$	280.534	276.166	275.342	272.585	272.570
Mg2-O1	279.565	277.424	278.812	278.064	278.446
Mg2-$O2^1$	280.029	284.137	284.548	271.283	279.125
Mg2-$O2^2$	279.102	279.115	280.707	280.175	280.763
Mg3-O1	257.437	266.870	266.666	278.846	280.128
Mg3-O2	289.456	287.862	295.008	284.069	284.466
TE[a]	6498.947	6515.077	6520.819	6522.142	6524.570

[a] The **TE** was the total bond energy.

from Fig. 9 that τ_f values are consistent with the changing trend of total bond energy, which means that the τ_f values are shifted toward zero. The higher the bond energy, the lower the bond strength. The radius of W^{6+} is smaller than that of Nb^{5+}, and the bond length of W–O bond is smaller than that of Nb–O bond. With the increase of the amount of

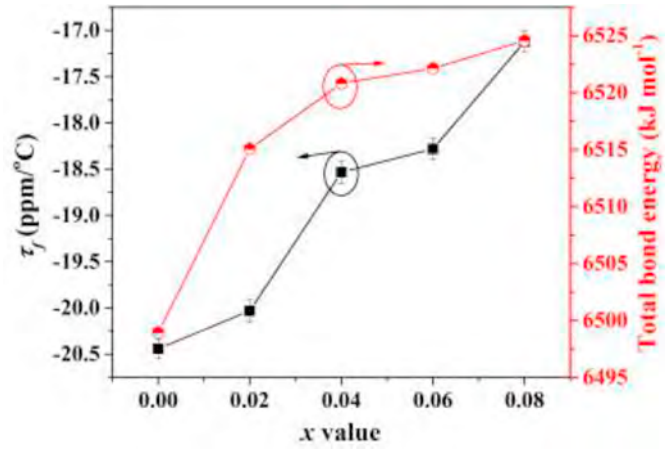

Fig. 9. The τ_f values and bond energy of $Li_3Mg_2(Nb_{1-x}W_x)O_{6+x/2}$ ($0 = x \le 0.08$) ceramics sintered at 1175 °C.

W^{6+}, the number of W–O bonds in oxygen octahedron increases, which improves the thermal stability of the samples.

4. Conclusions

The novel $Li_3Mg_2(Nb_{1-x}W_x)O_{6+x/2}$ ($0 \le x \le 0.08$) ceramics were successfully prepared through the solid-state reaction route. $Li_3Mg_2(Nb_{1-x}W_x)O_{6+x/2}$ ceramics formed a pure phase solid solution in the entire doping range. In addition, the variation of the dielectric constant and $Q \times f$ values of the sample with the sintering temperature was similar to the relative density. Further research showed that the dielectric constant was related to the ionic polarizability. The $Q \times f$ values were affected by the average bond valence and the density. The τ_f values depended on the total bond energy of $Li_3Mg_2(Nb_{1-x}W_x)O_{6+x/2}$ ceramics. In the end, $Li_3Mg_2(Nb_{0.94}W_{0.06})O_{6.03}$ ceramics sintered at 1175 °C for 6h had superior microwave dielectric properties, $\varepsilon_r \sim 15.82$, $Q \times f \sim 124{,}187$ GHz, $\tau_f \sim -18.28$ ppm/°C.

Declaration of competing interest

The authors declare that they have no known competing financial interests or personal relationships that could have appeared to influence the work reported in this paper.

Acknowledgments

This work was supported by Major Projects of Science and Technology in Tianjin (No. 18ZXJMTG00020) and the National Natural Science Foundation of China (No. 61671323).

Appendix A. Supplementary data

Supplementary data to this article can be found online at https://doi.org/10.1016/j.ceramint.2020.05.229.

References

[1] L.L. Yuan, J.J. Bian, Microwave dielectric properties of the lithium containing compounds with rock salt structure, Ferroelectrics 387 (2009) 123 12.

[2] M. Makimoto, S. Yamashita, K. Itoh, T. Sakurai (Eds.), Microwave Resonators and Filters for Wireless Communication: Theory, Design and Application, Springer Science & Business Media, Springer-Verlag Berlin Heidelberg, New York, 2001, pp. 1–7.

[3] D. Thomas, M.T. Sebastian, Temperature-compensated $LiMgPO_4$: a new glass-free low-temperature cofired ceramic, J. Am. Ceram. Soc. 93 (2010) 3828–3831.

[4] I.M. Reaney, D. Iddles, Microwave dielectric ceramics for resonators and filters in mobile phone networks, J. Am. Ceram. Soc. 89 (2006) 2063–2072.

[5] A.T. Vanderah, Talking ceramics, Science 298 (2002) 1182–1184.

[6] M.T. Sebastian, H. Jantunen, Low loss dielectric materials for LTCC applications: a review, Int. Mater. Rev. 53 (2008) 57–90.

[7] G.H. Chen, J.C. Di, H.R. Xu, M.H. Jiang, C.L. Yuan, Microwave dielectric properties of $Ca_4La_2Ti_{5-x}(Mg_{1/3}Nb_{2/3})_xO_{17}$ ceramics, J. Am. Ceram. Soc. 95 (2012) 1394–1397.

[8] H.F. Zhou, W. Wang, X.L. Chen, Y.B. Miao, X.B. Liu, L. Fang, F. He, Sintering behavior, phase evolution and microwave dielectric properties of thermally stable (1-x)Li_3NbO_4-x$CaTiO_3$ composite ceramic, Ceram. Int. 40 (2014) 2103–2107.

[9] X.L. Chen, H.F. Zhou, L. Fang, X.B. Liu, Y.L. Wang, Microwave dielectric properties and its compatibility with silver electrode of $Li_2MgTi_3O_8$ ceramics, J. Alloys Compd. 509 (2011) 5829–5832.

[10] Y.G. Zhao, P. Zhang, Microstructure and microwave dielectric properties of low loss materials $Li_3(Mg_{0.95}A_{0.05})_2NbO_6$ (A = Ca^{2+}, Ni^{2+}, Zn^{2+}, Mn^{2+}) with rock-salt structure, J. Alloys Compd. 658 (2016) 744–748.

[11] P. Zhang, L. Liu, M. Xiao, Y.G. Zhao, A novel temperature stable and high Q microwave dielectric ceramic in $Li_3(Mg_{1-x}Mn_x)_2NbO_6$ system, J. Mater. Sci. Mater. Electron. 28 (2017) 12220–12225.

[12] P. Zhang, L. Liu, M. Xiao, Microwave dielectric properties of high Q and temperature stable $Li_3(Mg_{1-x}Ni_x)_2NbO_6$ ceramics, J. Mater. Sci. Mater. Electron. 29 (2018) 5057–5063.

[13] C.F. Xing, J.X. Bi, H.T. Wu, Effect of Co-substitution on microwave dielectric properties of $Li_3(Mg_{1-x}Co_x)_2NbO_6$ ($0.00 \leq x \leq 0.10$) ceramics, J. Alloys Compd. 719 (2017) 58–62.

[14] M. Castellanos, J.A. Gard, A.R. West, Crystal data for a new family of phases, $Li_3Mg_2XO_6$: X = Nb, Ta, Sb, J. Appl. Crystallogr. 15 (1982) 116–119.

[15] P. Zhang, X.S. Wu, M. Xiao, Effect of Sb^{5+} ion substitution for Nb^{5+} on crystal structure and microwave dielectric properties for $Li_3Mg_2NbO_6$ ceramics, J. Alloys Compd. 766 (2018) 498–505.

[16] G. Wang, H.W. Zhang, X. Huang, F. Xu, G.W. Gan, Y. Yang, D.D. Wen, J. Li, C. Liu, L.C. Jin, Correlations between the structural characteristics and enhanced microwave dielectric properties of V-modified $Li_3Mg_2NbO_6$ ceramics, Ceram. Int. 44 (2018) 19295–19300.

[17] G. Wang, D.N. Zhang, X. Huang, Y. H Rao, Y. Yang, G.W. Gan, Y.M. Lai, F. Xu, J. Li, Y.L. Liao, C. Liu, L.C. Jin, V.G. Harris, H.W. Zhang, Crystal structure and enhanced microwave dielectric properties of Ta^{5+} substituted $Li_3Mg_2NbO_6$ ceramics, J. Am. Ceram. Soc. 103 (2019) 214–223.

[18] B. Zhang, L.X. Li, Investigation of chemical bonds in the ordered $Ba_3Zn(Nb_{2-x}Mo_x)O_{9+x/2}$ ceramics and its effects on the microwave performance, J. Eur. Ceram. Soc. 38 (2018) 4446–4452.

[19] P. Zhang, K.X. Sun, M. Xiao, Crystal structure, densification, and microwave dielectric properties of $Li_3Mg_2(Nb_{(1-x)}Mo_x)O_{6+x/2}$ ($0 \leq x \leq 0.08$) ceramics, J. Am. Ceram. Soc. 95 (2018) 4127–4135.

[20] P. Zhang, K.X. Sun, X.R. Mao, M. Xiao, Z.T. Zheng, Crystal structures and high microwave dielectric properties in Li^+/Ti^{4+} ions co-doped $Li_3Mg_2NbO_6$ ceramics, Ceram. Int. 46 (2020) 8097–8103.

[21] G. Wang, D.N. Zhang, J. Li, G.W. Gan, Y. H Rao, X. Huang, Y. Yang, L. Shi, Y.L. Liao, C. Liu, L.C. Jin, H.W. Zhang, Crystal structure, bond energy, Raman spectra, and microwave dielectric properties of Ti-doped $Li_3Mg_2NbO_6$ ceramics, J. Am. Ceram. Soc. (2020) 1–12 00.

[22] H. Wu, P.K. Davies, Influence of Non-stoichiometry on the structure and properties of $Ba(Zn_{1/3}Nb_{2/3})O_3$ microwave dielectrics: I. Substitution of $Ba_3W_2O_9$, J. Am. Ceram. Soc. 89 (2006) 2239–2249.

[23] B.W. Hakki, P.D. Coleman, A dielectric resonator method of measuring inductive capacities in the millimeter range, IEEE Trans. Microw. Theor. Tech. 8 (1960) 402–410.

[24] W.E. Courtney, Analysis and evaluation of a method of measuring the complex permittivity and permeability microwave insulators, IEEE Trans. Microw. Theor. Tech. 18 (1970) 476–485.

[25] R.D. Shannon, Revised effective ionic radii and systematic studies of interatomic distances in halides and chalcogenides, Acta Crystallogr. 32 (1976) 751–767.

[26] N. Ichinose, T. Shimada, Effect of grain size and secondary phase on microwave dielectric properties of $Ba(Mg_{1/3}Ta_{2/3})O_3$ and $Ba([Mg,Zn]_{1/3}Ta_{2/3})O_3$ systems, J. Eur. Chem. Soc. 26 (2006) 1755–1759.

[27] H.L. Pan, L. Cheng, H.T. Wu, Relationships between crystal structure and microwave dielectric properties of $Li_2(Mg_{1-x}Co_x)_3TiO_6$ ($0 \leq x \leq 0.4$) ceramics, Ceram. Int. 43 (2017) 15018–15026.

[28] R.D. Shannon, G.R. Rossman, Dielectric constants of silicate garnets and the oxide additivity rule, Am. Mineral. 77 (1992) 94–100.

[29] R.D. Shannon, Dielectric polarizabilities of ions in oxides and fluorides, J. Appl. Phys. 73 (1993) 348–366.

[30] C.L. Huang, W.R. Yang, P.C. Yu, High-Q microwave dielectrics in low-temperature sintered $(Zn_{1-x}Ni_x)_3Nb_2O_8$ ceramics, J. Eur. Ceram. Soc. 34 (2014) 277–284.

[31] D.M. Iddles, A.J. Bell, A.J. Moulson, Relationship between dopants, microstructure and the microwave dielectric properties of ZrO_2-TiO_2-SnO_2 ceramics, J. Mater. Sci. 27 (23) (1992) 6303–6310.

[32] R.T. Sandderson, Multiple and single bond energies in inorganic molecules, Inorg. Nucl. Chem. 30 (1968) 375–393.

[33] R.T. Sandderson, Chemical Bonds and Bond Energy, Academic Press, New York, 1971.

[34] R.T. Sandderson, Electronegativity and bond energy, J. Am. Chem. Soc. 105 (1983) 2259–2261.

[35] Y.R. Luo, Comprehensive Handbook of Chemical Bond Energies, CRC Press, 2007.